Transplanted optically-controlled stem cell-derived motor neurons restore muscle function

J. Barney Bryson[1], Carolina Barcellos Machado[2]*, Martin Crossley[2]*, Danielle Stevenson[2]*, Virginie Bros-Facer[1], Juan Burrone[2], Linda Greensmith[1,3,]†‡, Ivo Lieberam[2]†‡

[1]Sobell Department of Motor Neuroscience and Movement Disorders, University College London (UCL) Institute of Neurology, London, UK.

[2]Medical Research Council (MRC) Centre for Developmental Neurobiology, King's College London, Guy's Hospital Campus, London, UK.

[3]MRC Centre for Neuromuscular Diseases, UCL Institute of Neurology, London, UK.

*These authors contributed equally to this work.

† These authors contributed equally to this work.

‡ Corresponding author. E-mail: l.greensmith@ucl.ac.uk (L.G.); ivo.lieberam@kcl.ac.uk (I.L.)

Damage to the central nervous system caused by traumatic injury or neurological disorders can lead to permanent loss of voluntary motor function and muscle paralysis. Here, we describe an approach that circumvents central motor circuit pathology to restore specific skeletal muscle function. We generated murine embryonic stem cell–derived motor neurons that express the light-sensitive ion channel channelrhodopsin-2, which we then engrafted into partially denervated branches of the sciatic nerve of adult mice. These engrafted motor neurons not only reinnervated lower hind-limb muscles but also enabled their function to be restored in a controllable manner using optogenetic stimulation. This synthesis of regenerative medicine and optogenetics may be a successful strategy to restore muscle function after traumatic injury or disease.

Electrical stimulation of motor axons within peripheral nerves has been known to induce muscle contraction since Luigi Galvani's early experiments. In more recent times, phrenic

nerve pacing has been used clinically to control the function of the diaphragm, the major muscle involved in respiration, in some patients with high-level spinal cord injury (1) or amyotrophic lateral sclerosis (ALS) (2). However, peripheral nerves are composed of efferent motor axons as well as afferent sensory axons (which are unaffected in ALS). Functional electrical stimulation, which stimulates nerves indiscriminately, can thus cause considerable discomfort (3). Furthermore, functional electrical stimulation is ineffective if axon integrity is compromised because of injury or degenerative disease. Other strategies to replace lost motor neurons within the central nervous system include the use of embryonic stem cells (ESCs), but ESC-derived neurons do not always integrate into adult brain and spinal cord circuitry (4) and have difficulty overcoming molecular inhibitors of neuronal outgrowth (5) and extending axons across the barrier between the central and peripheral nervous system to reach the appropriate muscles (6).

It has previously been shown that motor neurons derived from ESCs can be engrafted into a peripheral nerve environment and successfully reinnervate denervated muscle (7). However, these engrafted cells are not connected to the descending inputs within the central nervous system that normally control motor function; therefore, their neural activity must be regulated by an artificial control system. Such engrafted ESC-derived motor neurons can be electrically stimulated (7), but this approach stimulates endogenous as well as engrafted neurons. In transgenic mice that express the light-sensitive ion channel channelrhodopsin-2 (ChR2) (8, 9) in endogenous motor neurons, it has been shown that the axons of these ChR2 motor neurons can be recruited by optical stimulation in a physiological and graded fashion, resulting in optogenetic control of muscle function (10). It has also been shown that viral expression of ChR2 in motor neurons of adult rats can enable optical stimulation of muscle function (11). In this study, we tested whether expression of ChR2 in ESC-derived motor neurons engrafted into a denervated peripheral nerve (i) confers optically regulated control of muscle function, without interfering with endogenous motor signals or afferent sensory axons, and (ii) enables physiological recruitment of motor units.

We generated genetically modified ESC-derived motor neurons that express both ChR2, to enable optical stimulation, as well as glial-derived neurotrophic factor (Gdnf), a neurotrophic factor that promotes long-term motor neuron survival (see supplementary materials and methods). To develop such ESCs suitable for in vivo engraftment of ESC motor neurons, we stably transfected an established mouse ESC clonal cell line that already carried the motor neuron–specific reporter Hb9::CD14-IRES-GFP (GFP, green fluorescent protein) (12) with a photoreceptor transgene that is expressed regardless of cell type, CAG::ChR2-YFP (YFP, yellow fluorescent protein), and with the neurotrophin-expressing CAG::Gdnf transgene. Embryoid bodies derived from CAG:ChR2-YFP/Gdnf ESCs, which express ChR2-YFP in all cells including motor neurons (Fig. 1A), were differentiated in vitro using an established protocol (13, 14). CAG::ChR2-YFP/Gdnf motor neurons also produce Gdnf (Fig. 1B), which improves their long-term survival in vitro (Fig. 1C). When cultured on an ESC-derived astrocyte feeder layer (fig. S1), ChR2 motor neurons mature electrically over a period of 35 days, until they fire trains of action potentials in response to optical stimulation and closely resemble adult motor neuron activity patterns induced by electrical stimulation (15) (Fig. 1D and fig. S2).

After developing these ChR2 motor neurons, we next established an in vivo model to assess the feasibility of restoring muscle function with optical control of the engrafted cells, using the sciatic nerve. Muscle denervation was induced by sciatic nerve ligation in adult mice. This procedure results in a complete initial denervation, followed by limited regeneration of endogenous axons through the ligation site, thereby creating a partially denervated environment resembling the partial muscle denervation of early-stage ALS (fig. S3). Three days post-ligation, embryoid bodies containing ChR2 motor neurons were engrafted distal to the ligation into the tibial and common peroneal branches of the sciatic nerve. Histological analysis revealed that the engrafted ChR2 motor neurons not only survive for at least 35 days in the peripheral nerve environment (Fig. 2A), but also mature morphologically to resemble adult spinal motor neurons and express the mature motor neuron marker choline acetyltransferase (Fig. 2B). Immunodetection of ChR2-YFP, using an antibody to GFP,

demonstrates that ChR2 is localized to the membrane of motor neurons, whereas direct detection of GFP versus YFP fluorescent signals reveals that Hb9-driven GFP expression is virtually absent in ChR2 motor neurons that have matured in vivo for 35 days (figs. S4 and S5). Additionally, ChR2 motor neurons extended large numbers of axons (Fig. 2C) distally toward both anterior [tibialis anterior (TA) and extensor digitorum longus (EDL)] and posterior [triceps surae (TS)] lower hind-limb muscles when grafted into the specific branches of the sciatic nerve that innervate these muscles. Engrafted ChR2 motor neuron axons, which grow alongside regenerating endogenous (YFP-negative) motor axons, are mostly myelinated (Fig. 2D). Histological analysis also revealed robust reinnervation of muscle fibers by ChR2 motor neurons, although the neuromuscular junctions exhibited hallmarks of inactivity, including poly-innervation as well as collateral and terminal axonal sprouting (16) (Fig. 2E), most likely because these motor neurons were inactive in vivo until stimulated by the external optical signal. Nevertheless, quantification of all end plates within a whole TS muscle revealed that 14.7% were innervated by YFP-positive ChR2 motor neurons axons after 35 days (Fig. 2F). Moreover, we observed YFP-positive neuromuscular junctions in both fast-twitch and slow-twitch regions of the TS, indicating that ChR2 motor neurons can innervate different muscle types. Therefore, this time point (35 days) was used in subsequent experiments to establish whether the transplanted ChR2 motor neurons were indeed functional and responsive to optical stimuli in vivo.

In anesthetized animals, we used isometric muscle tension physiology to examine the contractile responses elicited from TA, EDL, and TS (data summarized in table S1) muscles after optical stimulation of the exposed sciatic nerve using finely controlled pulses of 470nm blue light generated by a light-emitting diode (LED) unit and delivered via a light-guide to the graft site (Fig. 3A and movie S1). Short-duration (14ms) light pulses were able to induce submaximal twitch contractions in muscles innervated by transplanted ChR2 motor neurons (Fig. 3B), whereas high-frequency illumination (40 to 80Hz) induced tetanic muscle contraction (Fig. 3C) that can be repeated in a highly reproducible manner (Fig. 3D). Quantification of

these contractile responses demonstrated that the ratio of tetanic to twitch force was 3.09 ±0.52 and 2.34 ±0.33 for TA and EDL muscles, respectively (Fig. 3E), similar to normal values in uninjured animals.

Because nerve ligation enables regeneration of some endogenous motor axons, it was possible to directly compare the properties of these endogenous axons with those of the grafted ChR2 motor neurons by electrical nerve stimulation, which activates both populations of axons. This comparison demonstrated that the proportionate increase between twitch and tetanic stimuli after electrical stimulation was similar to that of optical stimulation [3.07 ±0.5 and 2.96 ±0.3 for TA and EDL muscles, respectively) (table S1)], although maximal force generation induced by optical stimulation of ChR2 motor neurons was weaker in comparison with electrical recruitment of both ChR2-expressing and endogenous motor neurons (12.2% of electrically induced force for TA and 12.3% for EDL). It is likely that this reduced force output of muscle fibers innervated by ChR2 motor neurons reflects the 35-day period of inactivity preceding optical stimulation, as indicated by the findings of the histological analysis of these muscles, which showed the presence of axonal sprouting and poly-innervated end plates, characteristic features of inactive muscles (16). Sustained optical stimulation in vivo would probably lead to reinforcement of these neuromuscular junctions and a corresponding increase in force output. Analysis of muscle contractile characteristics also revealed that the latency to peak twitch contraction from initiation of the electrical trigger to the LED unit, or direct stimulation of the nerve, was identical for both optical and electrical stimulation (Fig. 3F). This finding indicates that the nerve conduction velocities were similar for both types of stimulation and supports the histological findings showing that axons of ChR2 motor neurons are myelinated (Fig. 2D). Additionally, the contraction rate—that is, the time from initiation of muscle contraction to peak contraction—was also very similar (Fig. 3G) for both forms of stimulation. Repetitive trains of optical or electrical stimuli (40Hz, 250ms duration, every 1s) were delivered for a period of 180s to investigate the fatigue characteristics of the reinnervated muscles, which normally have a fast-twitch, fatigable phenotype. The results showed that

muscle fibers innervated by grafted ChR2 motor neurons were fatigue-resistant, in contrast to muscle fibers activated by electrical stimulation (Fig. 3H). Again, this probably reflects the prolonged period of inactivity of ChR2 motor neurons before optical stimulation.

Simultaneous activation of all motor neurons innervating a specific muscle would result in inefficient spasmodic contraction and muscle fatigue. It is therefore important that motor neurons are recruited physiologically, according to their activation threshold, to generate a graded muscle contraction that is proportionate to the intended force output. Activation threshold is normally determined by motor neuron soma size (17), but in the case of optogenetic activation of motor neurons, axonal diameter and intermodal distance are also important factors (10, 18).With this in mind, it was important to determine whether grafted ChR2 motor neurons could also be recruited in a graded manner by optical stimulation to induce physiological motor-unit recruitment, where smaller motor units are recruited before larger motor units. To test this, the illumination intensity of the LED was varied from 0.8 to 8mW/mm^2, which resulted in stochastic increases in muscle contractile force, demonstrating that different motor units could be recruited according to their optical activation threshold (Fig. 3I). This technique also enabled us to count the number of individual motor units innervating a given muscle, which for the TA muscle was 15 ±3.03. Furthermore, by comparing optical and electrical nerve stimulation, we found that grafted ChR2 motor neurons accounted for ~50% of all motor units (Fig. 3J). Moreover, the motor-unit counts enabled us to calculate the average motor-unit force (Fig. 3K), which, after optical stimulation, was found to be 0.21 ±0.04g and 0.16 ±0.05g for TA and EDL muscles, respectively. Combined recruitment of endogenous and ChR2 motor neuron axons by electrical stimulation resulted in average motor unit force values of 0.67 ±0.04 g and 0.59 ±0.34g for TA and EDL muscles, respectively, consistent with normal motor-unit force (0.62g).

In this study, we show that ChR2 motor neurons can be successfully transplanted into a peripheral nerve, where they can survive and extend axons that not only replace lost endogenous motor axons but also reinnervate denervated muscle fibers. Moreover, these

transplanted ChR2 motor neurons can be selectively activated by 470nm light, in a controlled manner to produce graded muscle contractions. Major challenges still remain before this approach can be established as an effective clinical intervention: These obstacles include the development of an implantable optical stimulator, such as that shown by Towne et al. (11), and a means to encapsulate the grafted cells. Additionally, incorporation of sensitive, red-shifted channelrhodopsin variants, such as ReaChR (19), rather than ChR2 would abrogate potential cellular toxicity associated with short-wavelength light (20).

These results show that through the use of a synthesis of regenerative medicine and optogenetics, it is possible to restore specific motor nerve functions. Although this study is largely a proof-of-principle study, it is possible that with further development this strategy may be of use in conditions where muscle function is lost—for example, after traumatic injury or neurodegenerative disease.

References and Notes

1. W. W. Glenn, M. L. Phelps. Diaphragm pacing by electrical stimulation of the phrenic nerve. *Neurosurgery* 17, 974–984 (1985).
2. R. P. Onders, et al. Complete worldwide operative experience in laparoscopic diaphragm pacing: results and differences in spinal cord injured patients and amyotrophic lateral sclerosis patients. *Surg. Endosc*. 23, 1433–1440 (2009).
3. B. Gernandt. Pain Conduction in the Phrenic Nerve. *Acta Physiol. Scand.* 12, 255–260 (1946).
4. S. C. Zhang. Embryonic stem cells for neural replacement therapy: prospects and challenges. *J. Hematother. Stem Cell Res.* 12, 625–634 (2003).
5. M. T. Filbin. Myelin-associated inhibitors of axonal regeneration in the adult mammalian CNS. *Nat. Rev. Neurosci*. 4, 703–713 (2003).
6. J. M. Harper, et al. Axonal growth of embryonic stem cell-derived motoneurons in vitro and in motoneuron-injured adult rats. *Proc. Natl. Acad. Sci.* U.S.A. 101, 7123–7128 (2004).
7. D. C. Yohn, G. B. Miles, V. F. Rafuse, R. M. Brownstone. Transplanted mouse embryonic stem-cell-derived motoneurons form functional motor units and reduce muscle atrophy. *J. Neurosci.* 28, 12409–12418 (2008).
8. G. Nagel, et al. Channelrhodopsin-2, a directly light-gated cation-selective membrane channel. Proc. *Natl. Acad. Sci.* U.S.A. 100,13940–13945 (2003).
9. E. S. Boyden, F. Zhang, E. Bamberg, G. Nagel, K. Deisseroth. Millisecond-timescale, genetically targeted optical control of neural activity. *Nat. Neurosci.* 8, 1263–1268 (2005).
10. M. E. Llewellyn, K. R. Thompson, K. Deisseroth, S. L. Delp. Orderly recruitment of motor units under optical control in vivo. Nat. Med. 16, 1161–1165 (2010).
11. C. Towne, K. L. Montgomery, S. M. Iyer, K. Deisseroth, S. L. Delp. Optogenetic control of targeted peripheral axons in freely moving animals. *PLOS ONE* 8, e72691 (2013).

12. C. B. Machado, et al. Reconstruction of phrenic neuron identity in embryonic stem cell-derived motor neurons. *Development* 141, 784–794 (2014).

13. H. Wichterle, I. Lieberam, J. A. Porter, T. M. Jessell. Directed differentiation of embryonic stem cells into motor neurons. *Cell* 110, 385–397 (2002).

14. M. Peljto, J. S. Dasen, E. O. Mazzoni, T. M. Jessell, H. Wichterle. Functional diversity of ESC-derived motor neuron subtypes revealed through intraspinal transplantation. *Cell Stem Cell* 7, 355–366 (2010).

15. L. Carrascal, J. L. Nieto-Gonzalez, W. E. Cameron, B. Torres, P. A. Nunez-Abades. Changes during the postnatal development in physiological and anatomical characteristics of rat motoneurons studied in vitro. *Brain Res. Brain Res. Rev.* 49, 377–387 (2005).

16. W. J. Thompson. Activity and synapse elimination at the neuromuscular junction. *Cell. Mol. Neurobiol*. 5, 167–182 (1985).

17. E. Henneman. Relation between size of neurons and their susceptibility to discharge. *Science* 126, 1345–1347 (1957).

18. J. Tønnesen. Optogenetic cell control in experimental models of neurological disorders. *Behav. Brain Res*. 255, 35–43 (2013).

19. J. Y. Lin, P. M. Knutsen, A. Muller, D. Kleinfeld, R. Y. Tsien. ReaChR: a red-shifted variant of channelrhodopsin enables deep transcranial optogenetic excitation. *Nat. Neurosci*. 16, 1499–1508 (2013).

20. P. E. Hockberger, et al. Activation of flavin-containing oxidases underlies light-induced production of H2O2 in mammalian cells. *Proc. Natl. Acad. Sci. U.S.A.* 96, 6255–6260 (1999).

Acknowledgments: We thank T. Keck, D. Kullman, and G. Schiavo for constructive feedback on the manuscript and the Thierry Latran Foundation for supporting this study. I.L. is funded by the Medical Research Council (G0900585), the Biotechnology and Biological Sciences Research Council (G1001234), King's Health Partners, and the Association Française contre les Myopathies. L.G. is the Graham Watts Senior Research Fellow, funded by The Brain Research Trust, and is supported by the European Community's Seventh Framework Programme (FP7/2007-2013). J.B. is a Wellcome Trust Investigator. The data reported in this paper are tabulated in the supplementary materials. We declare no conflicts of interest. I.L., C.B.M., M.C., and D.S. developed and characterized ESCs, prepared EBs, and purified motor neurons; M.C. and J.B. performed in vitro physiology; J.B.B. performed surgery, in vivo physiology, and histology and drafted the manuscript; V.B.-F. and D.S. assisted with surgery and histology; and L.G. and I.L. developed the original concept, designed and oversaw the study, and revised the manuscript.

Figure 1 | Expression of Gdnf in ChR2$^+$ESC-MNs enhances survival and enables them to mature electrically *in vitro*. (A) Embryoid bodies derived from CAG::ChR2-YFP/Gdnf transgenic ESCs and parental controls stained for the pan-motor neuron marker Isl1/2. GFP and YFP signals were detected by direct fluorescence. **(B)** Confocal images of MACS sorted ESC motor neurons derived from CAG::ChR2-YFP (MACS, magnetic-activated cell sorting) and CAG::ChR2-YFP/Gdnf ESCs immunostained for Gdnf and GFP/YFP. **(C)** Survival analysis of sorted CAG::ChR2-YFP and CAG::ChR2-YFP/Gdnf ESC motor neurons (MNs) (200 cells per well) plated on ESC astrocytes at indicated time points. CAG::ChR2-YFP motor neurons were cultured with (10 ng/ml) or without recombinant Gdnf (two replicates, analysis of variance with Bonferroni correction, *P < 0.25). Error bars indicate SEM. One representative of three separate experiments is shown. Wt, wild type. **(D)** Optogenetic stimulation (blue bars) of CAG::ChR2-YFP/Gdnf ESC motor neurons cultured on ESC astrocytes. Scale bars in **(A)** and **(B)**, 50 mm.

Figure 2 | Robust axonal growth and reinnervation of distal muscles following engraftment of ChR2$^+$ESC-MNs. (A) Image montage of a whole nerve and muscle section showing ChR2 motor neuron cell bodies at the graft site and axon projection (dashed lines indicate approximate trajectory). Scale bar, 500µm. **(B)** Confocal image of engrafted ChR2 motor neurons immunolabeled for choline acetyltransferase (ChAT; left image) and GFP and/or YFP (merged image at right). Scale bar, 50µm. **(C)** Confocal image of longitudinal and transverse common peroneal nerve sections showing both ChR2 motor neurons and endogenous axons. Scale bar, 50µm. **(D)** Confocal images of engrafted ChR2 motor neuron axons showing myelination. Scale bar, 50µm. **(E)** Confocal z-stack of ChR2 motor neuron axon terminals innervating multiple neuromuscular junctions within the TS muscle. Arrows indicate pre-terminal collateral sprouting, arrowheads denote terminal sprouting, and the asterisk indicates an endogenous motor axon. Scale bar, 50µm. **(F)** Two-dimensional projection image of a TS muscle showing proportion of neuromuscular junctions (NMJs) innervated by engrafted ChR2 motor neurons, relative to the total number of end plates

present [labeled with a-bungarotoxin (aBTx)]. Quantification is shown below. Representative images shown here are compiled from *n*=4 engrafted nerves from three separate experiments.

Figure 3 | Restoration of muscle function, in a highly controlled manner, using optical stimulation of engrafted ChR2^{+}ESC-MNs *in vivo*. (A) Schematic showing optical stimulation and isometric muscle tension recordings. EB, embryoid body. Representative twitch **(B)**, tetanic **(C)**, and repetitive tetanic **(D)** contraction traces obtained from the TA muscle, induced by optical stimulation. Blue line, muscle force; red line, electrical trigger signals sent to the LED unit. **(E)** Quantification of twitch and tetanic contraction of TA and EDL muscles. Time to peak contractile force, from initiation of the electrical trigger to the LED unit **(F)** or from the initiation of muscle contraction **(G)**, is shown alongside direct electrical nerve stimulation (*n*-values represent optical/electrical stimulation, respectively, compiled from four separate experiments). **(H)** Representative fatigue traces from TA muscles (different animals) produced by optical (top) or electrical (bottom) stimulation for 180s. **(I)** Representative TA muscle optical stimulation motor-unit number estimate trace. The asterisk indicates square-wave trigger voltage to the LED unit and oscilloscope trigger. **(J)** Motor-unit number quantification of TA and EDL muscles after optical versus electrical stimulation. **(K)** Analysis of average motor-unit force. The dashed line indicates the normal EDL value. All error bars indicate SEM.

Figure 1:

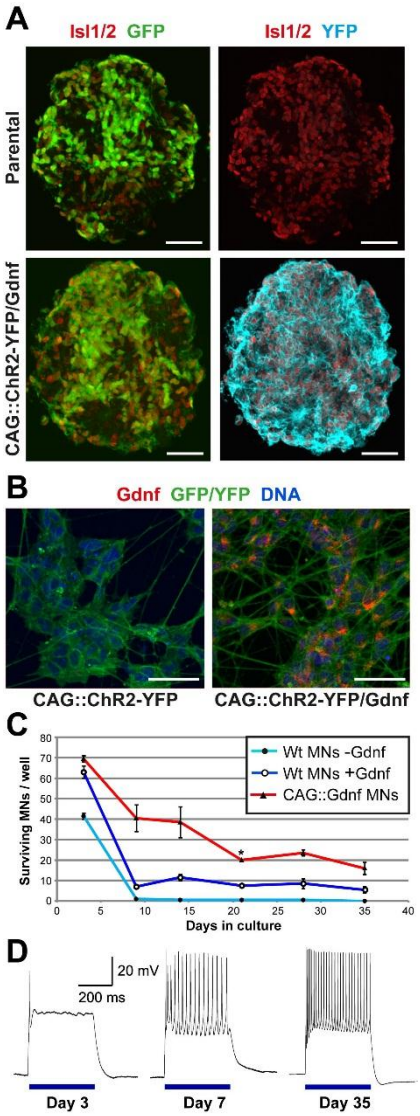
A
Isl1/2 GFP
Isl1/2 YFP
Parental
CAG::ChR2-YFP/Gdnf
B
Gdnf GFP/YFP DNA
CAG::ChR2-YFP
CAG::ChR2-YFP/Gdnf
C
Wt MNs -Gdnf
Wt MNs +Gdnf
CAG::Gdnf MNs
Surviving MNs / well
Days in culture
D
20 mV
200 ms
Day 3
Day 7
Day 35

Figure 2:

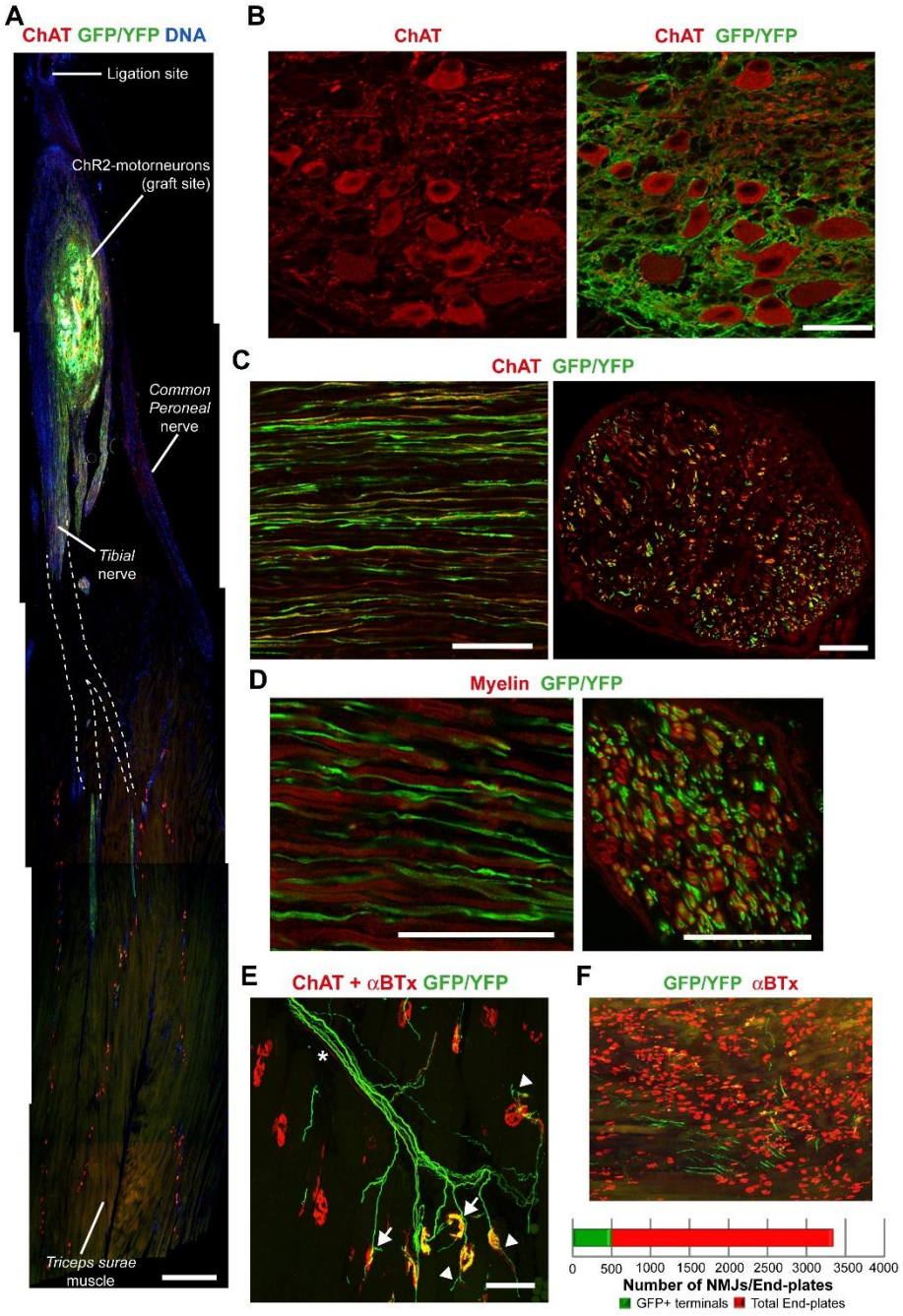
A
ChAT GFP/YFP DNA
Ligation site
ChR2-motorneurons
(graft site)
Common
Peroneal
nerve
Tibial
nerve
Triceps surae
muscle
B
ChAT
ChAT GFP/YFP
C
ChAT GFP/YFP
D
Myelin GFP/YFP
E
ChAT + αBTx GFP/YFP
F
GFP/YFP αBTx
0 500 1000 1500 2000 2500 3000 3500 4000
Number of NMJs/End-plates
GFP+ terminals
Total End-plates

Figure 3:

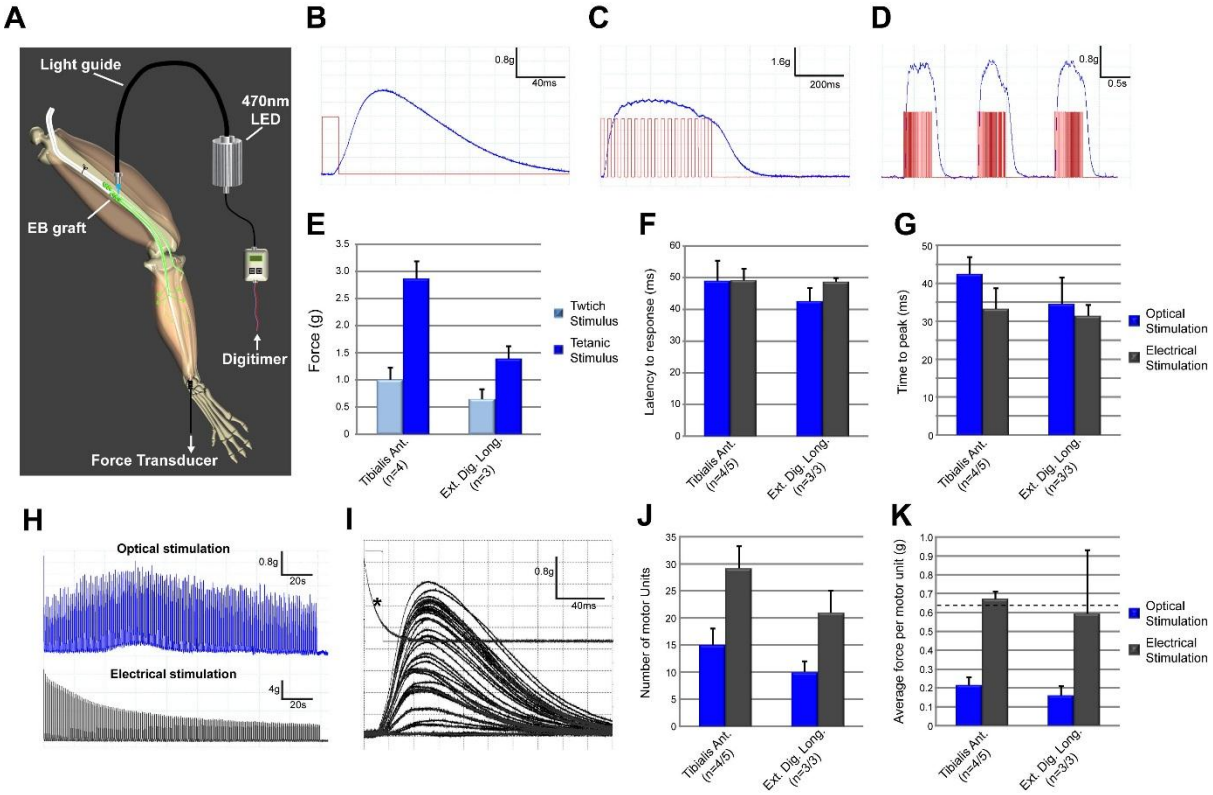
A
Light guide
470nm
LED
EB graft
Digitimer
Force Transducer
B
0.8g
40ms
C
1.6g
200ms
D
0.8g
0.5s
E
Force (g)
Twtich Stimulus
Tetanic Stimulus
Tibialis Ant. (n=4)
Ext. Dig. Long. (n=3)
F
Latency to response (ms)
Tibialis Ant. (n=4/5)
Ext. Dig. Long. (n=3/3)
G
Time to peak (ms)
Optical Stimulation
Electrical Stimulation
Tibialis Ant. (n=4/5)
Ext. Dig. Long. (n=3/3)
H
Optical stimulation
0.8g
20s
Electrical stimulation
4g
20s
I
0.8g
40ms
J
Number of motor Units
Tibialis Ant. (n=4/5)
Ext. Dig. Long. (n=3/3)
K
Average force per motor unit (g)
Optical Stimulation
Electrical Stimulation
Tibialis Ant. (n=4/5)
Ext. Dig. Long. (n=3/3)

SUPPLEMENTARY MATERIALS AND METHODS

Materials and Methods

Generation of stable ESC transfectants

Hb9::CD14-IRES-GFP 'bacterial artificial chromosome' transgenic ESCs (clone H14IG#13) (*12*) were equipped with a ubiquitously expressed ChR2^{H134R}-YFP transgene by stable transfection of a tol2L/R flanked expression vector consisting of the CAG promoter (*21*), followed by a 5' splice substrate, the ChR2-YFP gene, a bovine growth hormone (bGH) poly-adenylation sequence and a FRT-zeo-FRT resistance marker. 10 μg of the ptol2-CAG::ChR2-YFP/FRT-zeo construct and 20 μg of pCAGGS-Tol2-TP Tol2 transposase expression vector (kindly provided by Koichi Kawakami) were co-electroporated into H14IG#13 ESCs using a XCell GenePulser (Biorad) and the following settings: 'exponential mode', 240 V, 500 μF, 4 mm cuvettes. Recombinant ESC clones were selected with 50 μg/ml zeocin (Invitrogen) on mitomycin-C-(MMC) treated mouse embryonic fibroblasts, picked after 6 days based on YFP fluorescence, sub-cloned again, expanded and tested for the continued presence of the *Hb9::CD14-IRES-GFP* transgene by assessing their resistance to G418 (Invitrogen; 350μg/ml). Positive ESC clones were then screened for ChR2-YFP expression in motorneurons by in vitro differentiation, followed by fluorescence microscopy and electrophysiology. Clone Hb9::CD14-IRES-GFP#13/CAG::ChR2-YFP#1A (H14IG#13/CCRY#1A) was selected for further modification. This ESC sub-clone was then transfected with a transgene construct containing the CAG promoter, a 5' spice substrate, the mouse Gdnf gene, a bGH poly-adenylation sequence and a loxP-hygro-loxP resistance marker. The construct was flanked with piggyBAC terminal repeat sequences. 10 μg of the pPB-CAG::Gdnf/FRT-hygro construct and 20 μg of p3xP3-DsRed1-orf piggyBAC transposase expression vector (kindly provided by Malcolm J. Fraser) were co-electroporated into H14IG#13/CCRY#1A ESCs and recombinant ESC clones were selected with 150 μg/ml hygromycin (Invitrogen) on hygromycin-resistant

MMC-treated mouse embryonic fibroblasts, picked, expanded and screened for Gdnf expression by immunohistochemistry, and clone H14IG#13/CCRY#1A/CG#9G was chosen for subsequent experiments.

To produce an ESC clone that would specifically express the MACS-sortable reporter gene human CD14 in astrocytes, we prepared a transgene construct that consisted of the human GFAP (gfa2) promoter (*22*) (kindly provided by Michael Brenner), followed by a 5'splice substrate (*23*), the CD14 open reading frame, a bGH poly-adenylation sequence and a FRT-neo-FRT resistance marker (fig. S1A). This construct was flanked by tol2L/R recognition sequences (*24*). 10 µg of the ptol2-GFAP::CD14-I-GFP/FRT-neo construct and 20 µg of pCAGGS-Tol2-TP Tol2 transposase expression vector were co-electroporated into IB10 ESCs (*25*). Recombinant ESC clones were selected with 350 µg/ml G418 on G418-resistant MMC-treated mouse embryonic fibroblasts, picked, expanded and then screened for astrocyte-specific CD14 expression by in vitro differentiation, followed by immunohistochemistry. Clone GFAP::CD14#H6 (G14#H6) was selected for subsequent experiments. The tol2-insertion site in clone G14#H6 was mapped to the Ntm gene (chromosome 9.A4) by inverse PCR (*26*). We have been unable to identify the insertion sites in clone CCRY#1A/CG#9G.

ESC differentiation and MACS isolation of ESC-motorneurons and ESC-astrocytes

Motorneuron differentiation from *Hb9::CD14-IRES-GFP* ESCs (clone H14IG#13) and derivatives was performed as described by Peljto et al (*14*). ESC-motorneurons were isolated from dissociated day 5 embryoid bodies by anti-CD14 MACS enrichment as previously described (*12*). Astrocytes were generated and isolated from *GFAP::CD14* ESCs (clone G14#H6) as follows: Undifferentiated ESC colonies were dissociated with 0.25% Trypsin (Invitrogen) and grown in suspension in uncoated plastic dishes (Corning) to promote embryoid body formation. In the first 2 days, embryoid bodies were cultured in ADFNK medium (Advanced-DMEM/F12 (Invitrogen) and Neurobasal medium (Invitrogen) mixed at

1:1 ratio supplemented with 2 mM L-Glutamine, 0.1 mM 2-mercaptoethanol (Sigma), 10% knock-out serum replacement (Invitrogen), and 1x Penicillin/Streptomycin). For the subsequent 3 days the embryoid bodies were cultured in ADFNK medium supplemented with 1 μM retinoic acid (Sigma) and 0.5 μM Smoothened Agonist (SAG; Merck). At day 5 of differentiation, the embryoid bodies were re-plated onto 10cm tissue culture plates (Nunc) coated with GFR-matrigel (BD Biosciences) and cultured until day 12 in ADFNK medium. Then, the adherent embryoid bodies were washed once with PBS and dissociated with Accumax (Millipore; 6ml/plate) for 15 minutes at 37°C. The cell aggregates were broken into single cells by pipetting and washed three times (1200 rpm, 4 minutes) with L15 medium supplemented with 10 U/ml of DNase-I (Roche). The cells were then re-suspended in 2 ml of MACS buffer (PBS supplemented with 0.5% BSA (Sigma) and 10 U/ml of DNase-I) and passed through a 40 μm nylon strainer (BD Biosciences). The cells were centrifuged at 1200 rpm for 4 minutes, re-suspended in 200 μl of MACS buffer containing 5 μg/ml mouse anti-human CD14 (clone 26ic, ATCC), incubated at 10°C for 15 minutes, washed and then incubated with goat anti-mouse IgG MicroBeads (Miltenyi) diluted 1:10 in MACS buffer. After the secondary antibody incubation the cells were washed again, re-suspended in 600 μl of MACS buffer and applied to a MS magnetic column mounted in an OctoMACS magnet (Miltenyi). The column was washed three times with 500 μl MACS buffer, and the positive fraction eluted with 1 ml MACS buffer, following the manufacturer's instructions. In some experiments, the pre-MACs and eluate cell fractions were stained with anti-CD14 antibody conjugated to phycoerythrin (Millipore) and reanalysed using a Guava EasyCyte HT flow cytometer (Millipore). The astrocyte sort cell fractions were also cultured for 2 days on matrigel-coated 8-well permanox-slides (Nunc) in ADFNK medium and then fixed and analysed by immunocytochemistry.

Immunocytochemistry

Embryoid bodies were fixed in 4% paraformaldehyde/0.1M phosphate buffer for 30 minutes on ice, washed three times in PBS, equilibrated in 0.1M phosphate buffer/30% sucrose for 15 minutes, embedded in OCT and sectioned on a cryostat (Zeiss) at a thickness of 20 µm. Cultured cells were fixed for 20 minutes in 0.1M phosphate buffer /15% sucrose/4% paraformaldehyde and then washed with PBS three times. For CD14 detection on astrocytes, live cultured cells were stained with mouse anti-CD14 antibody (UCHM1, AbD Serotec; 10 µg/ml) for 30 minutes at RT in medium, washed five times with PBS and then fixed as described above. To detect Gdnf protein in cultured ESC-motor neurons, the cells were incubated with 10µg/ml brefeldin A (Sigma) in medium at 37°C for 1 hour prior to fixation. Antibody incubation was performed in PBS/0.1% TritonX-100/3% BSA using the following primary and secondary antibodies: rabbit anti-Isl1/2 (Epitomics, Burlingame, USA), rabbit anti-GFP (Invitrogen), goat anti-Gdnf (R&D Systems), rabbit anti-Gfap (DAKO), Alexa Fluor 568 donkey anti-goat IgG, Alexa Fluor 568 donkey anti-mouse IgG and Alexa Fluor 488 donkey anti-rabbit IgG (all secondary antibodies were obtained from Invitrogen). DNA counterstaining was carried out by adding 0.2 µM TOPRO3 (Invitrogen) to the secondary antibody labelling mix.

***In vitro* electrophysiology**

All electrophysiology data was obtained from visually targeted whole-cell patch-clamp recordings of ESC-motorneurons 3-35 days post sorting by MACS. The cultures were maintained for the duration of the patching protocol in an HBS extracellular solution (pH 7.4, ~280 mOsm) at room temperature that also contained (in mM): 136 NaCl, 2.5 KCl, 10 HEPES, 10 D-glucose, 2 $CaCl_2$ and 1.3 $MgCl_2$. Pipettes were pulled from borosilicate glass (out diameter 1.5 mm, inner diameter 1.17 mm, Harvard Apparatus), with a resistance of 3-6 MΩ, and were filled with an internal solution containing (in mM): 130 K-gluconate, 10 NaCl, 1 EGTA, 0.133 $CaCl_2$, 2 $MgCl_2$, 10 HEPES, 3.5 MgATP, 1 NaGTP. Recordings were acquired

with the Pulse software linked to a HEKA EPC10/2 amplifier. Signals were Bessel filtered at 10 kHz (filter 1), and 2.9 kHz (filter 2), digitized and sampled at 25-50 kHz (20-40 μs sample interval). Fast capacitance was compensated for in the on-cell configuration.

Analysis of action potential characteristics was carried out in current clamp mode from a resting membrane potential of approximately -60 mV. We provided 10 ms duration current steps of increasing amplitude (increments of 2, 5 or 10 pA), injected at the soma until the neuron reliably fired an action potential (V_m > 0 mV). The properties of the action potential were obtained from the first spike elicited for each neuron. For evaluation of firing behavior in response to long current injections, cells were typically held at around -60mV in current clamp mode and subjected to either 500ms duration current steps of increasing amplitude (increments of 10 or 20pA) or a 500 ms duration blue (~488nm at 170 mW/mm^2) light exposure provided by a shutter-controlled Xenon-arc lamp (Lambda-LS, Sutter Instruments, UK) with appropriate excitation filters (Chroma Tech. Corp., USA) but no neutral density filtering. Analysis of electrophysiological data was performed using custom-written functions in Matlab (Mathworks).

Surgical engraftment of EBs containing ChR2-motorneurons in ligated sciatic nerve

All procedures and experiments involving animals were carried out under License from the UK Home Office in accordance with the Animals (Scientific Procedures) Act 1986 (Amended Regulations 2012) and following ethical approval from UCL Institute of Neurology. Briefly, 8 week old female C57Bl6/J mice (Harlan Laboratories UK), n = 19, underwent sciatic nerve ligation: under deep anaesthesia (isoflurane) and using aseptic surgical conditions, the sciatic nerve was exposed and a 6-0 Ethicon^{TM} suture thread was tied tightly around the nerve in the upper thigh region; prophylactic analgesia was administered (buprenorphine, 0.05 mg/kg) and following wound closure animals were closely monitored and allowed to recover for 3 days (the refractory period during which axonal growth is inhibited by myelin debris). After 3 days,

the sciatic nerve was re-exposed, distal to the ligation site, and embryoid bodies (at Day 5 of the differentiation protocol, described above, which had been harvested and stored in ice-cold media prior to engraftment for <4 hrs) were injected into the tibial nerve and common peroneal nerve branches of the sciatic nerve using a 10µl Hamilton syringe with a customized 33G needle; typically 3-5 embryoid bodies were injected into each nerve branch in a volume of 0.5µl. Again, following wound closure, prophylactic analgesia was administered and recovery of animals was closely monitored during the post-surgical period. A subset of animals (n = 8) received grafts containing MACS-sorted, purified ChR2-motorneurons (approximately 10,000 cells/µl, injected in a volume of 0.5µl). These engrafted ChR2-motorneurons were capable of surviving *in vivo* for up to 35 d, however, the relatively small number of axons (compared to EB grafts) led to limited muscle innervation, therefore EB grafts were used for most experiments to provide the maximum innervation in this proof-of-principle study. EB engrafted mice (n = 11) and purified ChR2-motorneuorns engrafted mice (n = 8, representative example shown in fig. S5) underwent histological analysis at varying intervals following engraftment to determine survival and axonal growth and myelination of ChR2-motorneurons, and to determine muscle fibre innervation, as described below. *N*-values reflect data presented in this paper, rather than development of this strategy; only a subset of animals (n = 5) underwent optical/electrical nerve stimulation and physiological muscle recording (see below). Additionally, since the outcome measure of this study was unequivocal, randomization and blinding of groups was not necessary.

Immunohistochemistry

Animals were euthanized with an overdose of pentobarbital sodium (140mg/kg), and tissue was immediately removed; whole sciatic nerve (including tibial nerve and common peroneal nerve branches) were carefully dissected, maintaining connection to the triceps surae muscle to obtain a whole muscle/nerve preparation; tibialis anterior and extensor digitorum longus

muscles were also removed. Tissue was fixed to a silicon mounting block, using insect pins, and then immersed in 4% paraformaldehyde in tris-buffered saline (TBS), and post-fixed for 2hrs at 4°C and then transferred to 20% sucrose solution, in TBS, for cryoprotection and incubated at 4°C overnight. Samples were then carefully mounted in O.C.T. (Tissue-Tek 4583) medium, within flat-bottomed aluminum foil moulds, maintaining the whole muscle/nerve preparation in a horizontal plane; the moulds were then frozen on dry-ice. Serial longitudinal frozen sections (20μm) were then cut from the entire tissue block using a Bright^{TM} crysostat and sections were mounted onto poly-lysine coated slides (VWR 631-0107). After being air-dried (>2hr at room temperature), sections were immunostained according to standard protocols; briefly, sections were washed 3x with TBS, blocked with 5% normal donkey serum (NDS) in TBS containing 0.2% triton-X100 (TBS+), and primary antibodies (see below) in 2% NDS, in TBS+ were applied to the sections and incubated overnight at room temperature. Sections were then washed 3x with TBS and secondary antibodies (see below) in 2% NDS, in TBS+ were then applied for 1hr at room temperature – note: where applicable, α-bungarotoxin-TRITC (Sigma T0195, used 1:500), Fluoromyelin^{TM} (Molecular Probes F34652, used 1:300), and DAPI (Sigma D9542; used 1:1,000) were mixed with secondary antibody solution. Finally, sections were washed 3x with TBS and the coverslips were mounted using fluorescent mounting medium (DAKO) and allowed to dry.

For 3-D reconstruction of serial sections from a whole TS muscle, low magnification images were acquired using a Leica DMR epiflourescence microscope, and images were montaged using photoshop and then compiled into an aligned stack and 3-D reconstruction was performed using Metamorph^{TM} software. For all other image acquisition a Zeiss LM710 laser scanning confocal microscope was used. Primary antibodies used were: Rabbit anti-GFP (Molecular Probes A-11122, used 1:500), Goat anti-Choline Acetyltransferase (Millipore, AB144P, used 1:100) and Cy3-conjugated mouse anti-glial fibrillary acid protein (GFAP; Sigma C9205, used

1:1,000). Secondary antibodies used were: donkey anti-goat-Alexa568 (Molecular Probes A-11057, used 1:500), donkey anti-rabbit-Alexa488 (Molecular Probes A-21206, used 1:500).

***In vivo* isometric muscle tension physiology using optical and electrical stimulation**

The remaining animals (n = 5) that had undergone ChR2-motorneuron engraftment were deeply anaesthetized using isoflurane and the right lower hind-limb muscles were prepared for physiological recording (at 35d post-engraftment), as previously described (*27*). Briefly, the distal tendons of the triceps surae, tibialis anterior and extensor digitorum longus muscles were exposed, severed and individually connected to a force transducer. The lower hind-limb was immobilized, and the sciatic nerve was exposed at the mid-thigh level, and the overlying muscles were retracted. A light guide, connected to a 470nm LED light source (CoolLED; pE-100-LG), was then positioned 10 mm above the exposed, intact sciatic nerve. The control unit of the LED light source was connected to a Digitimer D4030 unit via a TTL trigger, which enabled pulses of light to be delivered for precise durations ranging from 5-50 ms, which were either delivered individually, to elicit twitch muscle contractions, or as repetitive high frequency (10-100 Hz, 450 ms duration) illumination, to elicit tetanic muscle contraction. Since 40Hz optical stimulation (12.5 ms illumination, 12.5 ms dark, per cycle) elicited the maximal contractile response, this pulse duration and frequency were employed as the standard optical stimulation paradigm. Additionally, the light-intensity could also be varied between 0-100% (0-80mW/mm^2) using the LED control unit; maximal responses were observed at 10% (8mW/mm^2), therefore this was used as the upper limit when recording motor unit traces. For electrical stimulation, the light guide was removed, and the sciatic nerve was severed proximally and the distal nerve stump (containing the engrafted ChR2-motorneurons) was placed in contact with a platinum electrode, as previously described (*27*). All muscle responses (and TTL trigger pulses) were recorded via an oscilloscope using Picoscope^{TM} software.

Statistical analysis:

For motorneuron survival count analysis and comparison of optical versus electrical isometric muscle tension physiology recordings, One-way ANOVA analysis was performed at each time point (where applicable) and *Bonferroni* post-hoc correction for multiple testing was applied. Normal distribution was confirmed for each data set. All error bars shown represent S.E.M.

Additional References:

21. H. Niwa, K. Yamamura, J. Miyazaki, Efficient selection for high-expression transfectants with a novel eukaryotic vector. *Gene* 108, 193–199 (1991).

22. M. Brenner, W. C. Kisseberth, Y. Su, F. Besnard, A. Messing, GFAP promoter directs astrocyte-specific expression in transgenic mice. *J. Neurosci.* 14, 1030–1037 (1994).

23. T. Choi, M. Huang, C. Gorman, R. Jaenisch, A generic intron increases gene expression in transgenic mice. *Mol. Cell. Biol.* 11, 3070–3074 (1991).

24. M. L. Suster, K. Sumiyama, K. Kawakami, Transposon-mediated BAC transgenesis in zebrafish and mice. *BMC Genomics* 10, 477 (2009).

25. E. Robanus-Maandag, M. Dekker, M. van der Valk, M. L. Carrozza, J. C. Jeanny, J. H. Dannenberg, A. Berns, H. te Riele, p107 is a suppressor of retinoblastoma development in pRb-deficient mice. *Genes Dev.* 12, 1599–1609 (1998).

26. K. Kawakami, T. Noda, Transposition of the *Tol2* element, an *Ac*-like element from the Japanese medaka fish *Oryzias latipes*, in mouse embryonic stem cells. *Genetics* 166, 895–899 (2004).

27. J. B. Bryson, C. Hobbs, M. J. Parsons, K. D. Bosch, A. Pandraud, F. S. Walsh, P. Doherty, L. Greensmith, Amyloid precursor protein (APP) contributes to pathology in the SOD1G93A mouse model of amyotrophic lateral sclerosis. *Hum. Mol. Genet.* 21, 3871–3882 (2012).

Extended Data

Extended Data Table 1 | Summary of data from *in vivo* isometric muscle tension physiology recordings obtained using optical and electrical stimulation. Summary of data from 3 separate experimental groups, showing optical stimulation values in blue boxes and electrical stimulation values in grey boxes. Data represents average values +/- S.E.M. (shown in parentheses); *n*-values for each muscle indicated in left-hand column; *,**,** denotes MU number estimate and MU Force data obtained from *n* = 2, 4 and 3 separate recordings, respectively.

	Twitch (g)	Tetanus (g)	Twitch : Tetanic Ratio	Twitch Latency (ms)	TTP (ms)	1/2 RT (ms)	MU number estimate	MU Force (g)
Triceps Surae (*n* =4)	1.6 (+/- 0.5)	1.4 (+/- 0.4)	1.3 (+/- 0.2)	1.3 (+/- 0.2)	43.5 (+/- 3.2)	39.5 (+/- 6.0)	15 (+/- 5.0)*	0.1 (+/- 0.01)*
Triceps Surae (*n* =3)	8.3 (+/- 2.4)	27.8 (+/- 7.3)	3.6 (+/- 0.3)	55 (+/- 4.3)	37.7 (+/- 3.1)	39 (+/- 10.2)	N/A	N/A
Tibialis Anterior (*n*=5)	1.0 (+/- 0.1)	2.4 (+/- 0.3)	3.1 (+/- 0.3	3.1 (+/- 0.3)	42.5 (+/- 3.4)	59 (+/- 8.6)	15 (+/- 1.5)**	0.2 (+/- 0.02)**
Tibialis Anterior (*n*=5)	6.4 (+/- 0.7)	19.3 (+/- 1.0)	3.1 (+/- 0.3)	49.2 (+/- 2.1)	33.3 (+/- 1.6)	27.7 (+/- 1.9)	29.2 (+/- 1.8)	0.7 (+/- 0.02)
Extensor Digitorum Longus (*n* = 3)	0.7 (+/- 0.1)	1.4 (+/- 0.1)	2.3 (+/- 0.2)	2.3 (+/- 0.2)	34.7 (+/- 1.9)	38 (+/- 3.8)	10 (+/- 1.2)	0.2 (+/- 0.03)
Extensor Digitorum Longus (*n* = 5)	3.4 (+/- 0.5)	11.4 (+/- 0.2)	3.0 (+/- 0.2)	48.7 (+/- 0.6)	31.5 (+/- 0.9)	29.5 (+/- 0.6)	21 (+/- 2.3)***	0.6 (+/- 0.19)***

Extended Data Figure legends:

Extended Data Figure 1 | Magnetic enrichment of GFAP::CD14^{+} astrocytes from ESC differentiation cultures (a) Schematic representation of the GFAP::CD14 transgene construct used to generate stable mouse ESC lines. 5'S: 5' splice substrate; pA: polyadentylation site; tol2R/tol2L: Tol2 transposase recognition sites. **(b)** The histogram shows flow cytometric analysis of anti-CD14 MACS enrichment of dissociated day 12 ESC differentiation cultures. Blue: pre-MACS; red: MACS eluate. **(c)** Pre-MACS, flow through and eluate from the anti-CD14 MACS-enrichment were plated out on matrigel-coated tissue culture dishes, cultured for 3 days and then fixed and immunostained for CD14 and Gfap. The percentages of CD14^{+} cells (counted from three representative images each) are shown in the upper right corners. Scale bar = 50µm

Extended Data Figure 2 | Responses of ESC-derived MNs to electrical and optical stimulation *in vitro.* Representative current clamp traces from ChR2+ESC-MNs stimulated

with a 500ms current injection (top row), or a 500ms blue light pulse (blue bar; bottom row). All cells were cultured on monolayers of ESC-derived astrocytes expressing a constitutively active Gdnf transgene (see Extended Data Fig. 1). Cells were held at -60mV for recording. **(b)** Analysis of single action potentials of ChR2+ESC-MNs stimulated with a 10ms current injection in current clamp mode. Mean Rm values for 3, 7, 21 and 35 DIV MNs were 581.2 (n=6), 369.4 (n=4), 109.6 (n=8) and 76.3MΩ (n=10) respectively. **(c)** The output from ChR2+ESC-MNs was obtained from step-wise current injections of increasing amplitude (500 ms) at the soma in current clamp mode (example voltage traces shown in (a)). The graph represents the number of action potentials fired during a 500 ms current pulse (expressed as mean frequency) as a function of input current density. Note how immature ChR2+ESC-MNs (DIV 3-7) cannot sustain high frequency firing compared to more mature neurons (DIV 21-35). By DIV 35, neurons can fire at average rates that go beyond 50Hz. The gradual shift of input-output curves to the right (along the input current axis) as development progresses is likely due to the increase in Cm and decrease in Rm as neurons grow and mature. Cells were stimulated from a resting membrane potential of -60mV. DIV = Days *in vitro.* All error bars show ± S.E.M.

Extended Data Figure 3 | Engrafted purified ChR2+ESC-MNs survive *in vivo* and avoids the presence of dividing cells. Confocal images of engrafted GFP/YFP-positive EBs (+35d *in vivo*) showing the presence of MNs immunostained for ChAT **(a)** and astrocytes, immunostained for GFAP **(b)**; both MN somas and astrocytes remained confined to the graft-site and did not migrate within the nerve (data not shown). **(c)** Image of engrafted purified ChR2+ESC-MNs showing that they can survive for the same duration (+35d) as ChR2+ESC-MNs within EBs, and that all GFP/YFP immunostaining co-localizes with ChAT, indicating the absence of other contaminating cell populations. Scale bars = 50μm.

Extended Data Fig 1

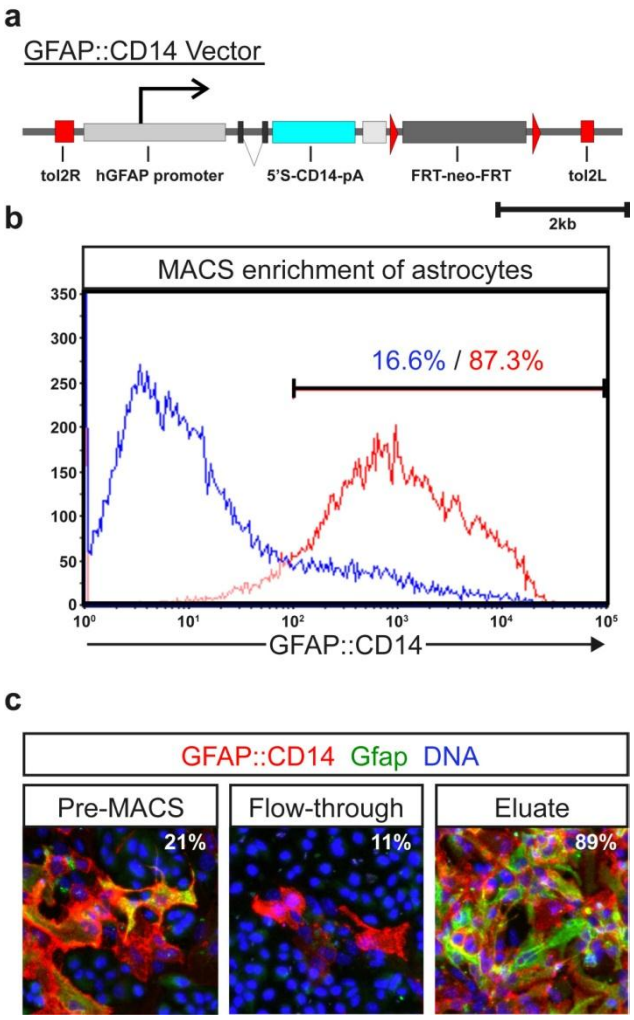

Extended Data Fig 2

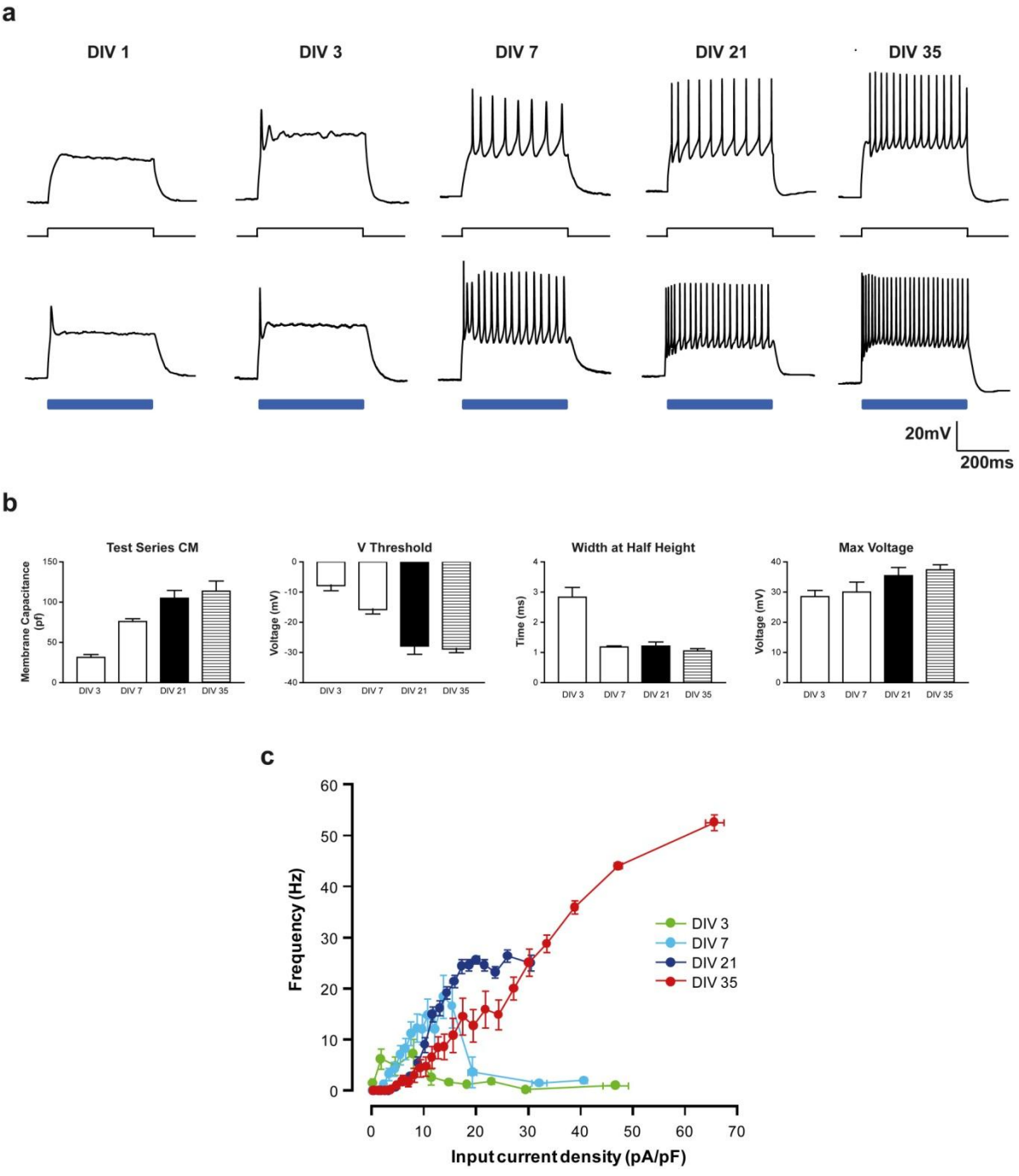

Extended Data Fig 3